IOP Publishing Physica Scripta
Phys. Scr. 95 (2020) 055306 (9pp) https://doi.org/10.1088/1402-4896/ab784e

Preequilibrium strength in light heavy-ion induced reactions up to 7 MeV/nucleon

Rinku Prajapat, Moumita Maiti, Deepak Kumar[1] and Amit Chauhan

Department of Physics, Indian Institute of Technology Roorkee, Roorkee-247667, India

E-mail: moumita.maiti@ph.iitr.ac.in

Received 6 October 2019, revised 16 February 2020
Accepted for publication 20 February 2020
Published 2 March 2020

Abstract

The crux of this article is to analyze the contribution of the preequilibrium reaction process to the production of residues in the low energy heavy-ion reactions. The production cross-sections of a few radionuclides produced through the $3n$-emission channel have been measured from the ^{7}Li-, ^{11}B- and ^{12}C-induced reactions in the ^{89}Y and ^{93}Nb targets within the energy range of ~2.4–6.4 MeV/nucleon. The measured excitation functions have been analyzed by comparing them with the statistical nuclear reaction models, based on the equilibrium and preequilibrium reaction mechanisms, in the framework of ALICE91 and EMPIRE3.2.2. The result shows that the mixing of equilibrium and preequilibrium emission of light or cluster particles is essential for the better reproduction of the measured cross-section data. Variation of the preequilibrium fractions with derived energy parameters has also been demonstrated.

Keywords: fusion reactions, cross-section, preequilibrium strength, stack-foil technique, weakly and tightly bound projectiles

(Some figures may appear in colour only in the online journal)

1. Introduction

In heavy-ion collisions, kinetic energy and angular momentum brought by a projectile could be dissipated in several internal degrees of freedom after the interaction with a target nucleus, and the process leads to form a highly excited composite system. The composite system then evolves towards the thermal equilibrium (EQ), and the light particles or clusters, which could not sustain in the energy relaxation process, are emitted carrying considerable energy and angular momentum before the thermal equilibration has reached. These particles, which move with relatively higher energy compared to those emitted from the compound nucleus, are known as preequilibrium particles; the process is called preequilibrium (PEQ) reaction. PEQ emissions occur on a much faster time scale compared to the EQ emissions. The emission rate of these particles or nucleons confides the mean-field interaction between the colliding partners. Interpretation of projectile and target interaction at zero temperature, i.e. Fermi energy is provided by the two-body interaction between the nucleons of the composite system, and the rearrangement of energy between these nucleons takes place through the coupling between the translational momentum per nucleon of the colliding nuclei with their internal momentum [1]. The particle emissions in the PEQ process play a significant role in enhancing the production of residues in light and heavy-ion reactions [2–14]. The study gives an encyclopedic idea of those processes that occur during the deexcitation of nonequilibrated hot rotating nuclei created after a projectile-target interaction. A detailed review of these data mentioned that apart from the non-fusion and fragmentation processes, a significant amount of preequilibrated particles also emit from the composite system before attaining an equilibrium state.

Efforts have been made to estimate the production of residues through the PEQ process theoretically as well as experimentally within ~10–20 MeV/nucleon energy range [15–19]. Nandy *et al* [15] demonstrated the angular distribution of preequilibrated light particles using the kinematics of nucleon-nucleon scattering and satisfactorily reproduced the experimental data. The illustration by Maiti *et al* [16] suggested that the theoretical estimation of PEQ emission within the framework of the exciton model and geometry dependent hybrid model in different reaction codes,

[1] Present address: Flerov Laboratory of Nuclear Reactions, JINR, Moscow region, Dubna-141980, Russia.

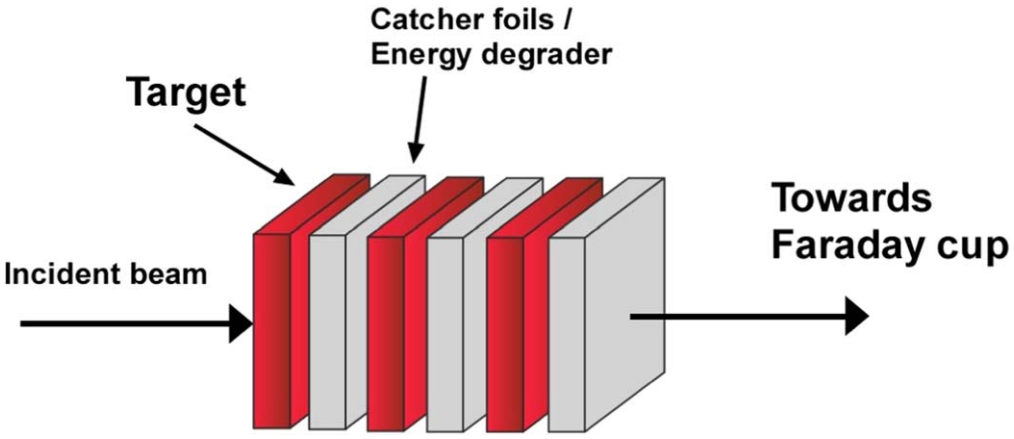

Figure 1. A schematic diagram of the target-catcher foil arrangement used for the presently studied reactions.

like TALYS and ALICE91, play a crucial role in emphasizing the production window of some medically relevant radionuclides. The excitation functions from $^{12}C+^{181}Ta$ and ^{187}Au, and $^{16}O+^{165}Ho$ and ^{181}Ta reaction reported by Cavinato *et al* [17] have mentioned that PEQ followed by EQ processes successfully reproduce the experimental data within or below 10 MeV/nucleon energy range. It has been explained by Birattari *et al* [18] that there is a reasonable change in the mean-field interaction between the nucleons with the change of energy, and they also have estimated the strength of PEQ emission in $^{12}C+^{103}Rh$ within 20 MeV/nucleon energy. Sharma *et al* examined the PEQ emission from the ^{12}C and ^{16}O induced reactions on some medium mass targets within ~7 MeV/nucleon energy range [4]. Acharya *et al* [7] measured the excitation functions from $^{14}N+^{103}Rh$ reaction up to 400 MeV energy and concluded that by including the multi-nucleon and cluster emissions in initial stages during the PEQ emissions provide satisfactory results with experimental data using Hybrid Monte Carlo simulation(HMS) model. In this series, a study of complete-incomplete fusion (CF-ICF) and PEQ reactions have been carried out using the $^{12}C+^{197}Au$ reaction below 10 MeV/nucleon energy [8]. The study of low energy heavy-ion reactions has also gained our interest to disentangle various nuclear reaction phenomena such as EQ-PEQ and CF-ICF in the past few years [2, 3, 19–33].

Besides heavy-ion reactions, a considerable amount of data exists in the literature on the nucleon, and light-ion induced reactions, which might be useful for the production of radionuclides application, and to test the emerging statistical reaction codes. PEQ models are necessary to reproduce the experimental data in the light-ion reactions such as *n* and *p* reaction on the medium mass targets, ^{32}S, ^{64}Zn, ^{67}Zn, ^{89}Y, ^{90}Zr, and ^{153}Eu [9]. Amanuel *et al* [10] illustrated that a combination of EQ and PEQ is mandatory for the best reproduction of experimental data in $\alpha+^{93}Nb$ reaction using ALICE91. Avrigeanu *et al* [11] reported the effect of optical model potential, shell effects, and continuum effect on the cross-section and compared the measured excitation functions with theoretical models in *n*-induced reaction on ^{55}Mn, and $^{63,65}Cu$ at energies up to 40 MeV. On the other hand, Parashari *et al* [12] have shown the comparison of experimental data with the recently updated code TALYS1.9 and concluded that the addition of PEQ emission contribution is essential for light-ion induced reaction towards the higher energy range.

The study of light heavy-ion reactions might be useful to optimize the production window of some medically relevant radionuclides such as ^{97}Ru (2.83 d), ^{101m}Rh (4.34 d), ^{103}Pd (16.99 d) and $^{207-210}At$ (1.63–8.1 h), ^{183}Os (13 h) via EQ and PEQ mechanisms [21–38]. Further, it is worthy of mentioning that heavy-ion reaction data are hardly available below 10 MeV/nucleon in the literature to understand the dynamics of EQ-PEQ processes. Therefore, it is appropriate to estimate the PEQ emissions from various heavy-ion reactions to understand its dependence on the various degrees of freedom. With this aim, we have measured the excitation functions (EFs) of the residues produced in the $^{7}Li+^{89}Y$, $^{7}Li+^{93}Nb$, $^{11}B+^{89}Y$, $^{11}B+^{93}Nb$ and $^{12}C+^{89}Y$ reactions within ~2.4–6.4 MeV/A energy range. In the present work, we have reported a set of new cross-section data of ^{93m}Mo produced in the $^{7}Li+^{89}Y$ reaction, and a systematic analysis of the PEQ emissions observed in the 3*n*-emission channel from those reactions.

2. Experimental details

The light heavy-ions such as ^{7}Li, ^{11}B, and ^{12}C ions were bombarded on the stack of self-supporting pure (99.9%) ^{89}Y and ^{93}Nb target foils at BARC-TIFR Pelletron facility, Mumbai, India, within 2.4–6.4 MeV/nucleon energy range in the laboratory frame of reference. A typical stack-foil arrangement shown in figure 1 was adopted. The target stacks were prepared by placing 2–3 target foils, where each target foil was backed by an aluminum catcher foil. The thickness of the Y and Nb target foils were between 0.84–3.9 mg cm^{-2} and 1.2–3.5 mg cm^{-2}, respectively, while the thickness of Al foils was between 1.5–3 mg cm^{-2}. The Al foils fulfill the purpose of energy degrader so that a suitable energy separation, beyond the uncertainty limit of two consecutive energy points, between the successive targets in an assembly could be achieved. Since the self-supporting metal foils (Y, Nb, and

Table 1. Nuclear spectroscopic data of the 3*n*-channel residues, and details of the reactions considered [46].

System	$E_C(c.m.)$[a] (MeV)	Energy range E_{lab} (MeV)	Residue	J^{π}	$T_{1/2}$	Decay mode (%)	E_γ (keV)	I_γ (%)
^{7}Li+^{89}Y	16.4	19–40	^{93m}Mo	$21/2^{+}$	6.85 h	IT[b](99.88),	263.05	57.4
						ϵ[c]+β^{+}(0.12)	684.69	99.9
^{7}Li+^{93}Nb	17.1	20–45	^{97}Ru	$5/2^{+}$	2.83 d	$\epsilon+\beta^{+}$(100)	215.7	85.6
							324.5	10.8
^{11}B+^{89}Y	26.6	27–59	^{97}Ru	$5/2^{+}$	2.83 d	$\epsilon+\beta^{+}$(100)	215.7	85.6
							324.5	10.8
^{11}B+^{93}Nb	27.8	30–63	^{101}Pd	$5/2^{+}$	8.47 h	$\epsilon+\beta^{+}$(100)	296.29	19.0
							590.44	12.06
^{12}C+^{89}Y	31.9	40–75	^{98}Rh	2^{+}	8.72 min	$\epsilon+\beta^{+}$(100)	652.6	97.0

[a] Coulomb barrier.
[b] Isomeric transition.
[c] Electron capture.

Al) were prepared by hand-rolling technique, the thickness of the foils was not uniform for all the foils. In order to include a wide energy range in the excitation functions, at least five stacks of target-catcher foil assembly were irradiated for each reaction varying the bombarding energy, so that overlap in energy point be achieved to crosscheck the residual cross-section from different sets of irradiation. The beam energy degradation in each target and catcher foil was calculated by the Monte-Carlo-simulation based SRIM (Stopping and Range of Ions in Matter) code [39]. The beam energy at a particular target is the average of the incident and outgoing energy. The beam energy degradation in a foil (dE/dx) is proportional to its thickness and inversely proportional to the bombarding energy. Hence, a larger thickness of the foils was chosen for the high energy irradiations, and the number of target-catcher foils was varied accordingly to avoid significant beam divergence during the experiment. Therefore, although the precise thickness of the foils and their numbers are known for each irradiation, a range for those are mentioned here.

At the end of bombardment (EOB), populated residues in each target foil were identified with the help of γ-ray spectrometry, and the spectra were recorded using a high-purity germanium detector attached with a PC operating with GENIE-2K software. The detector was precalibrated using ^{137}Cs (30.08 y) and ^{152}Eu (13.517 y) sources having known activity. The spectroscopic properties of the residues, and details of the reactions studied are tabulated in Table 1. The cross-section for each populated residues was measured using the activation formula. A detail description of the residual cross-section measurement is available in our previous reports [2, 32, 33].

The error propagated in the cross-section measurement was from (1) the determination of the target thickness of ~2%–5%, (2) the fluctuation in the beam flux was ~5%, (3) efficiency calibration of the detector ~2%, (4) statistical error in the peak area counts was negligible, (5) in the quest of minimizing the error, the dead time of the detector was kept $\leqslant$10% by adjusting the geometry of measurement, which is essentially the distance between detector and sample location. The calculated error associated with the measured cross-sections accounts for all those factors, and the measured data are presented here up to the 95% confidence level.

3. Model calculation: EMPIRE3.2.2 and ALICE91

EMPIRE3.2.2, the latest version of EMPIRE [40], has been used for the theoretical estimation of EQ and PEQ cross-sections for the evaluation of nuclear data. EMPIRE considers the Hauser-Feshbach (HF) formalism [41] with width fluctuation correction for compound evaporation (EQ), and the Exciton model with Iwamoto-Harda cluster emission model (EM) for the investigation of PEQ effect. The contribution of direct reactions has been considered in the framework of the coupled-channel approach for deformed nuclide, and DWBA approximation [42] for slightly deformed and spherical nuclei within this code. In order to contemplate the mean free path (MFP) between nucleon-nucleon scattering inside the nucleus, the MFP parameter ranges from 0.5 to 3.0. In any statistical model, the optimization of nuclear levels per MeV is an important tool for the prediction of the cross-sections. Therefore, EMPIRE considers different phenomenological nuclear level density models such as Gilbert-Cameron (GC) model [43], Generalized Super-fluid Model (GSM) [44] and Enhanced Generalized Super-fluid Model (EGSM) [45], etc. The GSM and EGSM consider the collective (rotational or vibrational) effects on the intrinsic level density that enhanced the theoretical cross-section values. EGSM deliberate the effect of high angular momentum as compared to GSM, which makes it more effective in heavy-ion collisions. In our present calculations, we have used the HF+EM with MFP parameter as 1.5, which is optimum value, and three different level density models, such as GC, EGSM, and GSM.

In ALICE91 [47], the EQ process is implemented employing the Weisskopf-Ewing (WE) model [48], and PEQ emission is estimated in the framework of hybrid- or geometry-dependent hybrid model (GDH) [49, 50]. It has various options for the level density like Fermi gas (FG), Kataria–Ramamurthy (KR) with shell correction, Ignatyuk, and Gilbert-Cameron (GC). Although there exist many input parameters to play, yet level density parameter $a = A/K$, where

Table 2. A list of default and opted parameters for the codes EMPIRE3.2.2 and ALICE91.

Parameter	EMPIRE (Default)	EMPIRE (Opted)	ALICE (Default)	ALICE (Opted)
EQ Model	Hauser-Feshback (HF)	HF	Weisskopf-Ewing(WE)	WE
PEQ Model	Exciton model (EM)	EM	Hybrid/Geometry dependent hybrid (GDH)	— GDH
Level density model	EGSM	EGSM, GSM, GCM	FG	FG
Mean free path parameter	0.5 to 3	1.5	0	0, 2 and 6
Level density parameter	Described in [3]	—	A/9	A/8, A/9, and A/11

A is mass number of the composite system, and K is a free parameter, initial exciton number n_0 ($n_p + n_h$), where n_p and n_h are the number of excited particles and holes, respectively, and MFP multiplier denoted by COST are sensitive to the estimation of residual cross-sections. In order to account for the difference between the calculated and actual MFP between the nucleons, an adjustable parameter COST is provided, MFP is multiplied by (COST+1) in this reaction code. MFP could be modified by adjusting the multiplier COST to reproduce the measured data. The value for this adjustable parameter COST is suggested between 1 to 10 by Blann and Musthafa *et al* [49, 51]. Many other parameters like *Q*-values and binding energies are taken from the recently updated Wang and Audi mass tables [52], whenever the masses are not available in the table, they are measured from the Myers-Swiatecki mass formula (Lysekil) [53]. The contribution of inverse reaction cross-section has been estimated within this code from the optical model, which utilizes the Bechhatti and Greenlees nucleus-nucleus optical model parameters [54]. In the present calculation, we have adopted the WE+GDH model and FG level density. Further, variation in the residual cross-sections has been studied by varying level density parameter $a = \mathrm{A/K\ MeV^{-1}}$ (K = 8, 9, and 11), and COST parameter (COST = 0, 2, and 6). A comprehensive list of the default parameters of these codes and the opted parameter for the calculation are tabulated in table 2.

4. Results and discussion

4.1. Analysis of excitation functions

To understand the dynamics of the reaction processes such as EQ and PEQ at the low-energy region, the cross-sections of the residues, ^{93m}Mo, ^{97}Ru, ^{97}Ru, ^{101}Pd, and ^{98}Rh, which are populated via 3*n*-channel from the ^{7}Li+^{89}Y, ^{7}Li+^{93}Nb, ^{11}B+^{89}Y, ^{11}B+^{93}Nb, and ^{12}C+^{89}Y reactions, respectively, have been measured and compared with the theoretical estimations from two reaction model codes, EMPIRE and ALICE, as depicted in figures 2 and 3. The theoretical estimations from EMPIRE, which includes the combined effect of EQ and PEQ processes in the framework of HF and EM models with three different level densities such as EGSM, GSM, and GC, grossly describe the measured data throughout the energy range for all the residues. Yet, EGSM more accurately reproduces the data in most cases, as shown in figure 2.

Figure 2(a) compares the production cross-section of ^{97}Ru from the ^{7}Li+^{93}Nb reaction, and that of ^{93m}Mo from ^{7}Li+^{89}Y reaction up to 45 MeV with EMPIRE. In the case of ^{97}Ru, EMPIRE with all three level density models (EGSM, GSM, and GC) reproduce the measured cross-sections after considering the EQ+PEQ models in the calculation. Yet, EMPIRE with EGSM shows the best match with the measured data for both the reactions. However, for ^{93m}Mo, EMPIRE with EGSM reproduces the data more precisely throughout the energy range, while the estimations with two other level densities show a good agreement with the measured data up to ∼30 MeV and start diverging from the measured data beyond it.

Figure 2(b) compares the measured excitation function of ^{97}Ru, ^{101}Pd, and ^{98}Rh produced from the ^{11}B+^{89}Y, ^{11}B+^{93}Nb [3] , and ^{12}C+^{89}Y reactions, respectively, with EMPIRE. The cross-sections of ^{97}Ru is well described by EMPIRE with GSM level density throughout the energy range, while predictions from the two other level densities (EGSM, and GC) reasonably agree with the measured data. Like other residues, EMPIRE with EGSM level density reasonably reproduces the ^{101}Pd cross-section data with slight underprediction in the high energy tail. Similarly, ^{98}Rh excitation function data [33] are better reproduced by the EGSM level density model using EMPIRE throughout the energy range.

Given the above analysis, it could be concluded that the admixture of EQ+PEQ models is necessary to reproduce the measured cross-sections of the 3*n*-channel residues from all the studied reactions. In a previous report, Kumar *et al* [2] also discussed the reproduction of ^{97}Ru from ^{7}Li+^{93}Nb reaction through the combination of HF+EM models with EGSM level density. Although the performance of EMPIRE has been excellent for the reactions reported here, the strength of the PEQ reaction process, called PEQ fraction (refer the next section), could not be estimated using EMPIRE, as it does not disentangle the EQ and PEQ cross-sections from the total (EQ+PEQ). Hence, we have used another statistical reaction code ALICE91, which could separate the EQ cross-section from the aggregate, to analyze the measured residual cross-sections.

Figure 3(a) reveals that the theoretical predictions from ALICE using WE model, which estimates only EQ emissions,

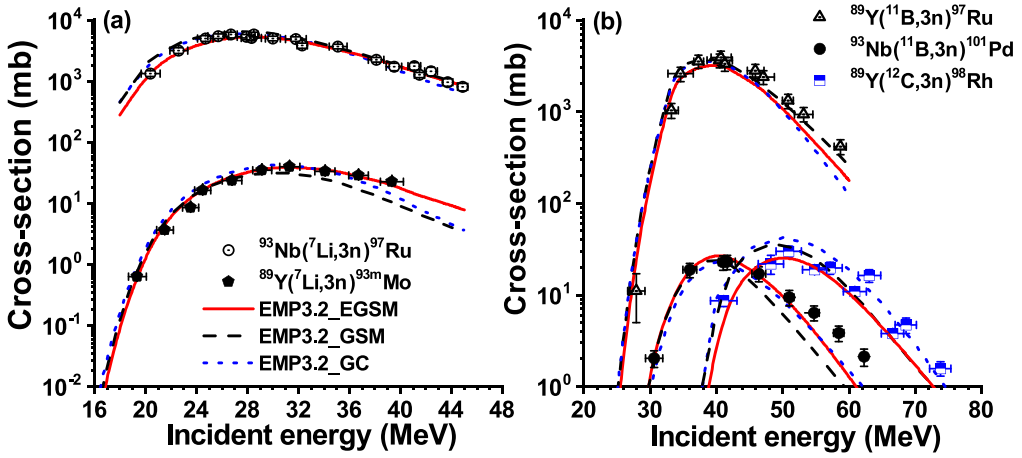

Figure 2. Comparison between the measured excitation function of (a) ^{97}Ru and ^{93m}Mo, (b) ^{97}Ru, ^{101}Pd, and ^{98}Rh with the theoretical predictions from EMPIRE3.2.2 (denoted EMP3.2). All the cross-sectional values are multiplied by 10 for ^{97}Ru, and 0.1 for ^{93m}Mo, ^{101}Pd, and ^{98}Rh.

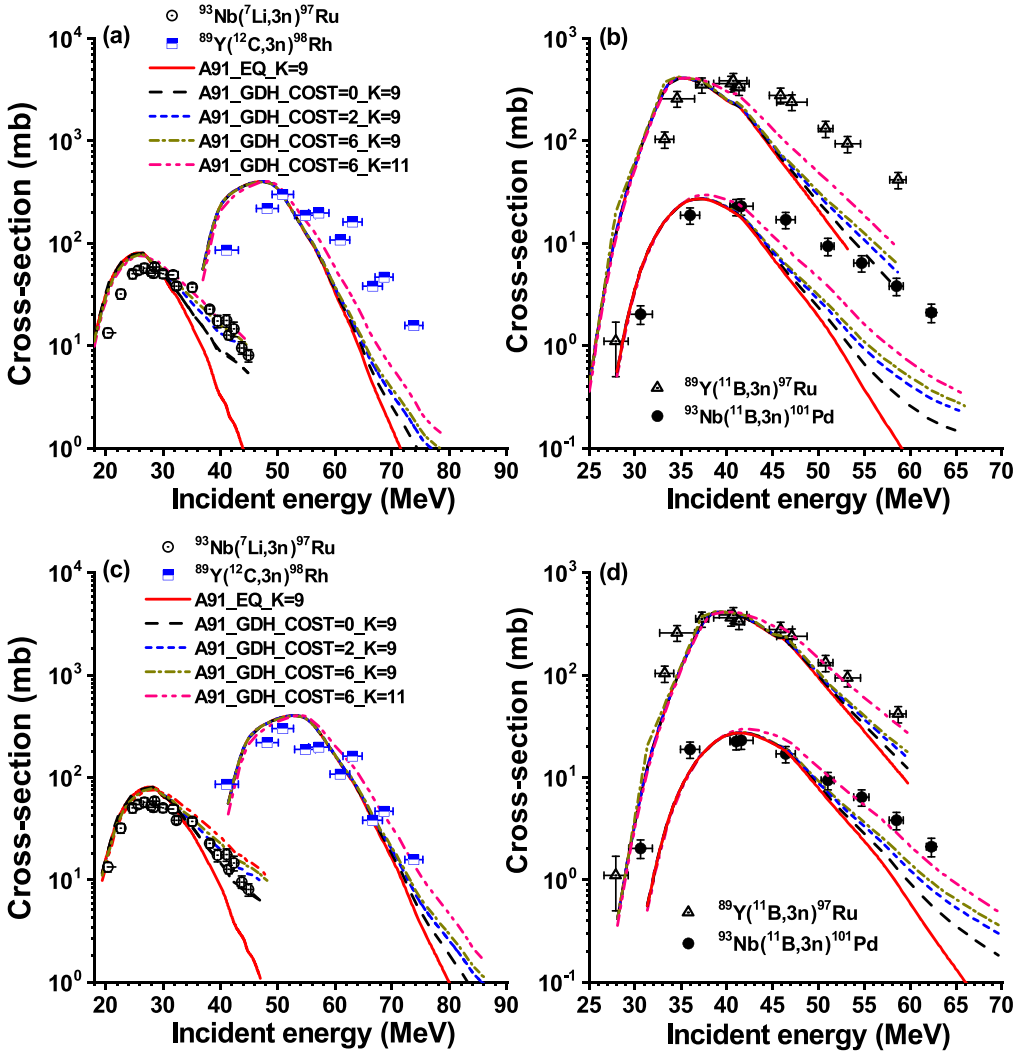

Figure 3. Comparison between measured excitation function of (a) ^{97}Ru and ^{98}Rh, (b) ^{97}Ru and ^{101}Pd, without E_{rot} energy correction, and (c) ^{97}Ru and ^{98}Rh, (d) ^{97}Ru and ^{101}Pd with E_{rot} energy correction in the theoretical predictions of ALICE91 (denoted as A91). The cross-sectional values are multiplied by 0.1 for ^{93}Nb(^{7}Li,3n)^{97}Ru and ^{93}Nb(^{11}B,3n)^{101}Pd.

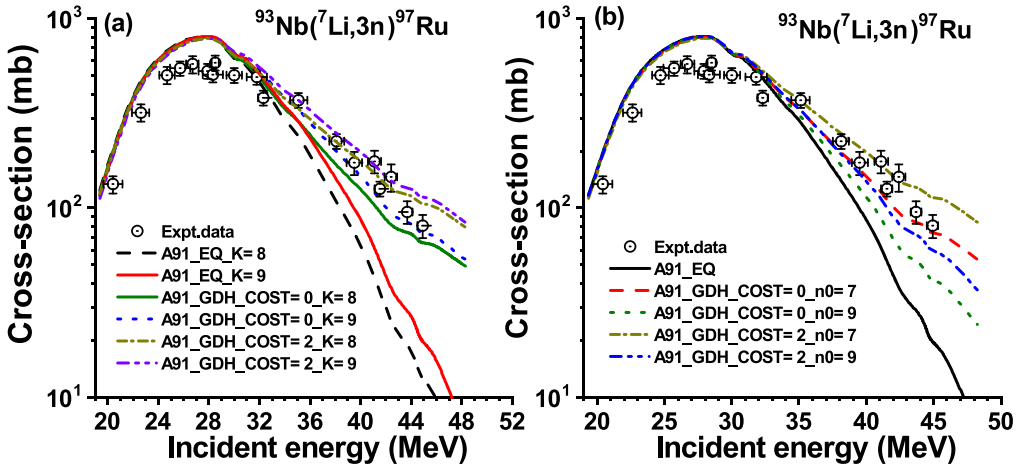

Figure 4. Comparison of measured and theoretical excitation function for ^{93}Nb(^{7}Li,3n)^{97}Ru reaction from ALICE91 (denoted as A91) with E_{rot} energy shift in the energy scale and the effect of (a) Parameter K = 8 and 9, COST = 0, 2 (b) Exciton number n_0 = 7 and 9, COST = 0, 2, with constant K = 9.

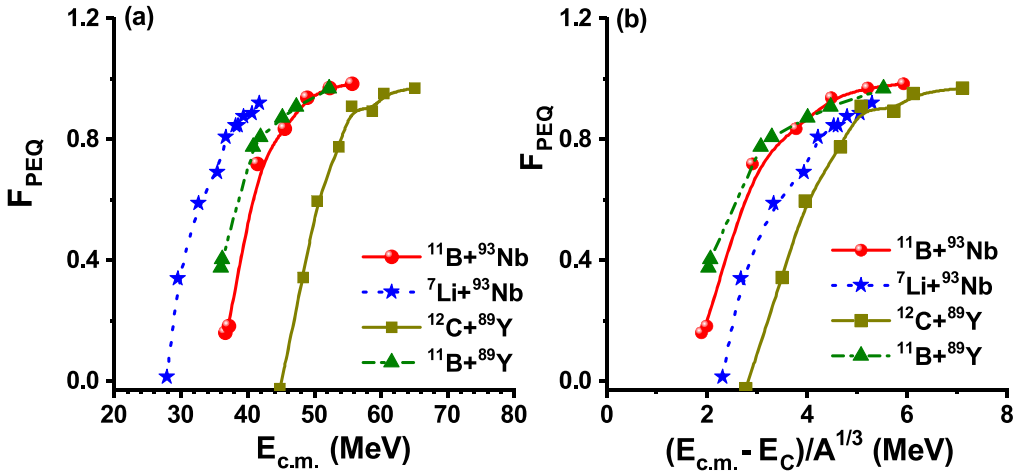

Figure 5. (a) Variation of F_{PEQ} with $E_{c.m.}$, (b) Variation of F_{PEQ} as a function of $(E_{c.m.}-E_C)/A^{1/3}$, E_C is the Coulomb barrier.

overpredict the measured cross-sections of ^{93}Nb(^{7}Li,3*n*)^{97}Ru reaction in the low-energy range (⩽30 MeV), and underpredict them beyond 30 MeV. The difference observed between the measured data and pure EQ emission estimated from the code in the higher energy range could be attributed to the PEQ emission of a few neutrons. We, therefore, have employed the combination of EQ and PEQ models (WE +GDH model) to reproduce the measured data. For the prediction of PEQ cross-sections, we have considered initial exciton number (total number of excited particles *p* and holes *h*), $n_0 = 7$ ($7p + 0h$) for ^{7}Li, and $n_0 = 11$ ($11p + 0h$) for ^{11}B, and $n_0 = 12$ ($12p + 0h$) for ^{12}C induced reactions; the MFP parameter, COST = 0, 2, and 6. The WE+GDH model with COST = 0 and K = 9, overpredict the measured data (<30 MeV) and underpredict them beyond ∼32 MeV; however, theoretical predictions (WE+GDH) with COST = 2, 6, K = 9, and COST = 6, K = 11, well reproduce the experimental data of ^{97}Ru within 30–50 MeV energy range and show overprediction below 30 MeV energy.

However, comparison of the measured excitation function of ^{89}Y(^{12}C,3*n*)^{98}Rh, ^{89}Y(^{11}B,3*n*)^{97}Ru, and ^{93}Nb(^{11}B,3*n*)^{101}Pd with ALICE91, as presented in figures 3(a) and (b), show that ALICE91 with pure EQ emission, and EQ+PEQ with different COST parameters with K = 9 and COST = 6, K = 11 consistently underpredict the measured data beyond ∼56 MeV for ^{98}Rh, beyond ∼40 MeV for ^{97}Ru and ^{101}Pd, and overpredict them below ∼52 and ∼40 MeV, respectively. Since ALICE91 does not estimate the cross-section of the isomeric states of the residue, no comparison has been made for the ^{89}Y(^{7}Li,3*n*)^{93m}Mo reaction with ALICE91.

It can be seen from figures 3(a), and (b) that the peak of the measured excitation functions constantly remains at higher energy as compared to those estimated from ALICE91. Since the angular momentum effect has not been considered in the WE model in ALICE91, the issue could be resolved by considering the rotational energy correction in ALICE91 calculations. A shift in incident energy by a factor of nuclear rotational energy could work for the possible correction. The rotational energy, E_{rot}, of a rigid-body is $\sim(M_p/M_t)E_{lab}$, where M_p/M_t is the ratio of projectile and target nucleus masses, and E_{lab} is the incident projectile energy in the

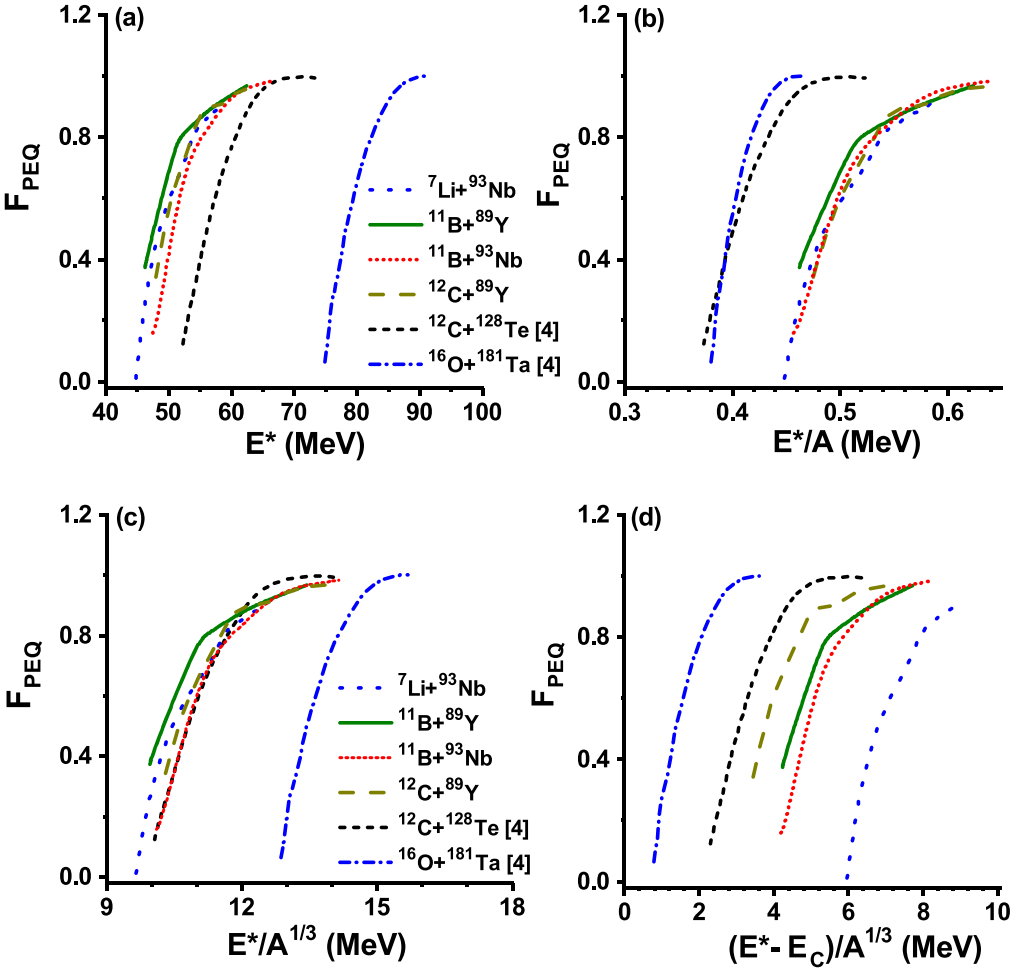

Figure 6. (a) Variation of F_{PEQ} as a function of (a) Excitaion energy of composite system E^* (b) Excitaion energy per nucleon of the composite system E^*/A, (c) Excitaion energy per peripheral nucleon of the composite system $E^*/A^{1/3}$, (d) Excitation energy in excess above the Coulomb barrier per peripheral nucleon of the composite system $(E^*\text{-}E_C)/A^{1/3}$.

laboratory frame [55]. Thus, the rotational energy corrected results from ALICE91, as portrayed in figures 3(c) and (d), show a fairly good match with the measured data using WE +GDH with COST = 6 and K = 11, except for the ^{93}Nb(^{7}Li,3n)^{97}Ru reaction. Therefore, the effect of variation of parameters such as K, n_0, and COST has been studied after considering the effect of rotational energy. As an example, the ALICE91 predicted excitation functions for the ^{93}Nb(^{7}Li,3n)^{97}Ru reaction using K = 8 and 9, n_0 = 7 and 9 (8*p*-1*h*), and COST = 0 and 2, as shown in figures 4(a) and (b), are compared with the measured data. The ALICE91 predictions with COST = 0, K = 9, and n_0 = 7 reproduce the measured data satisfactorily after considering the rotational energy shift.

It is evident from the present study that the observed difference between the measured data and estimated EQ emission towards the high energy range is mainly due to the PEQ emission of neutrons. At the same time, a little effect due to any other factor is also expected. Therefore, an analysis of the strength of the PEQ emissions has been described in the next section.

4.2. Analysis of PEQ strength fraction

The PEQ strength fraction (F_{PEQ}) estimates the contribution of PEQ emissions of light particles at relatively high energies. F_{PEQ} is defined as $(\sigma_{EQ+PEQ}\text{-}\sigma^{th}_{EQ})/(\sigma_{EQ+PEQ})$, where σ_{EQ+PEQ} is the measured cross-section of a residue that was populated by the EQ and PEQ processes, σ^{th}_{EQ} corresponds to the EQ cross-section of the residue calculated theoretically. The variation of F_{PEQ} has thus been estimated from the ^{7}Li-, ^{11}B-, and ^{12}C-induced reactions on ^{89}Y and ^{93}Nb considered in this study with the increasing energy in the center of mass frame ($E_{c.m.}$), as shown in figure 5(a). PEQ fraction sharply surges with increasing energy and reaches a saturation beyond specific energy, where the contribution of EQ emission becomes negligible. It is evident that the threshold of PEQ strength fraction is different for each reactions, PEQ starts from ∼28 MeV, ∼40 MeV, ∼42 MeV, and ∼52 MeV for ^{7}Li+^{93}Nb, ^{11}B+^{89}Y, ^{11}B+^{93}Nb, and ^{12}C+^{89}Y reactions, respectively, which possibly due to the variation in Coulomb barrier between two heavy colliding partners.

The early formulation of the EM could not reproduce the enhanced emissions from the nuclear surface; therefore, the hybrid model was introduced to provide a first-order

correction to the observed deficiency considering all the entrance channel impact parameters. Later, Blann and Vonach considered the diffuse nuclear surface properties into the PEQ formalism, in the GDH model [50]. Hence, to check the peripheral effect, which is correlated to the high impact parameter, on the PEQ emissions of light particles or clusters by eliminating the effect of Coulomb barrier, F_{PEQ} of all four systems has been plotted as a function of excess energy above the Coulomb barrier per unit peripheral nucleon of the composite systems, $(E_{c.m.}\text{-}E_C)/A^{1/3}$, where E_C is the Coulomb barrier in the center of mass frame, as presented in figure 5(b). Since all four systems that carry similar composite nuclear mass show similar F_{PEQ} systematic, it is not straightforward to draw a specific conclusion from this.

In the PEQ model, the excitation energy (E^*) plays a role in setting the limit on the emission of nucleon or cluster, and the amount of energy it carries from a composite nucleus. Thus, the variation of PEQ fraction with excitation energy had also been reported for both light- and heavy-ion induced reactions in the literature [4, 6, 49], including Blann's study on PEQ fraction for the α-induced reaction on ^{93}Nb [49]. Therefore, in the present study, variation of F_{PEQ} has been plotted as a function of excitation energy, and some other derived energy parameters such as excitation energy per nucleon (E^*/A), and per peripheral nucleon ($E^*/A^{1/3}$) as portrayed in figures 6(a), (b), and (c), respectively. Although the pattern or the trend of F_{PEQ} obtained from all four systems looks similar, they overlap considerably; hence no specific conclusion on the effect of entrance channel parameters could be described from those. However, it could be pointed out that E^*/A and $E^*/A^{1/3}$ are not the right parameters to analyze PEQ emissions.

Figure 6(d) describes the variation of F_{PEQ} eliminating the effect of the Coulomb barrier from E^*. Although F_{PEQ} for ^{7}Li-, ^{11}B-, ^{12}C-, and ^{16}O-induced reactions are somewhat clearly separated, as seen from figure 6(d), concluding the projectile effect would be unjustified due to the lack of similar data. A similar observation on the role of excitation energy to the PEQ emission was reported in [4] for the relatively large composite systems that included ^{12}C+^{128}Te and ^{16}O+^{181}Ta reactions, which have also been added with the relatively light systems considered in our study for the comparison, as depicted in figure 6. PEQ emission starts at lower $(E^*\text{-}E_C)/A^{1/3}$ value for the large composite systems as far as ^{12}C+^{128}Te and ^{16}O+^{181}Ta reactions are concerned, and it starts at higher excitation energy above the Coulomb barrier for the lighter composite systems, mass ranges between 100–104 in our study. This observation does not strictly apply to the projectile-target combination we have considered; instead, they represent mostly a group of reactions that produced almost similar composite masses from different projectile-target combinations. It might be possible that the excess energy liberated among the nucleons at the periphery of the composite system helps in PEQ emission of light particles, mostly nucleons. However, it appears that the mass number of the composite system might be a vital factor in PEQ emission apart from the type of projectile and the energy it carries.

5. Conclusion

This article demonstrates the measurement and analysis of the production cross-sections of ^{93m}Mo, ^{97}Ru, ^{97}Ru, ^{101}Pd, and ^{98}Rh populated via 3*n*-channel from the ^{7}Li+^{89}Y, ^{7}Li+^{93}Nb, ^{11}B+^{89}Y, ^{11}B+^{93}Nb, and ^{12}C+^{89}Y reaction, respectively. Hauser-Feshbach formalism and the exciton model reproduces the experimental data more accurately in the whole energy range, hence consideration of admixture of PEQ followed by EQ is necessary to explain the experimental data. The PEQ strength fraction (F_{PEQ}) increases with increasing projectile energy. However, the elimination of the effect of the Coulomb barrier from excitation energy and its normalization by the peripheral effect reveals that the PEQ emission starts at lower $(E^*\text{-}E_C)/A^{1/3}$ value for the large composite systems as compared to the lighter systems. However, the role of a projectile and the external energy it brings to the composite system should not be ignored in the study of the PEQ processes.

Acknowledgments

The authors gratefully acknowledge the help and cooperation received from the BARC-TIFR Pelletron team during the experiment. We thank Dr M Blann for the useful discussion on the model calculation. Research Grant No. CRG/2018/002354 from SERB(IN), Grant No. 03(1467)/19/EMR-II from CSIR(IN), and the research fellowships from the MHRD (IN), Government of India, are gladly acknowledged.

ORCID iDs

Rinku Prajapat https://orcid.org/0000-0003-3555-3126
Moumita Maiti https://orcid.org/0000-0001-9460-4347

References

[1] Brusati C, Cavinato M, Fabrici E, Gadioli E and Erba E G 1995 *Z. Phys.* A **353** 57
[2] Kumar D, Maiti M and Lahiri S 2016 *Phys. Rev.* C **94** 044603
[3] Kumar D and Maiti M 2017 *Phys. Rev.* C **95** 064602
[4] Sharma M K, Singh P P, Singh D P, Yadav A, Sharma V R, Bala I, Kumar R, Unnati, Singh B P and Prasad R 2015 *Phys. Rev.* C **91** 014603 and reference therein
[5] Shahid M, Kim K, Naik H, Zaman M, Kim G, Yang S C and Song T Y 2015 *Nucl. Instrum. Methods Phys. Res.* B **342** 158
[6] Sharma M K, Musthafa M M, Shuaib M, Kumar M, Sharma V R, Yadav A, Singh P P, Singh B P and Prasad R 2019 *Phys. Rev.* C **99** 014608
[7] Acharya J, Mukherjee S, Steyn G F, Singh N L and Chatterjee A 2016 *Phys. Rev.* C **93** 024608
[8] Vergani P, Gadioli E, Vaciago E, Fabrici E, Erba E G, Galmarini M, Ciavola G and Marchetta C 1993 *Phys. Rev.* C **48** 1815
[9] Aytekin H and Baldık R 2013 *Ann. Nucl. Energy* **53** 439
[10] Amanuel F K, Zelalem B, Chaubey A K, Agarwal A and Rizvi I A 2011 *Chin. J. Phys.* **49** 884 https://www.scopus.

com/record/display.uri?eid=2-s2.0-80054022368&origin=inward
[11] Avrigeanu M, Chuvaev S V, Filatenkov A A, Forrest R A, Herman M, Koning A J, Plompen A J M, Roman F L and Avrigeanu V 2008 *Nucl. Phys.* A **806** 15
[12] Parashari S, Mukherjee S, Nayak B K, Makwana R, Suryanarayana S V, Naik H and Sharma S C 2018 *Nucl. Phys.* A **978** 160
[13] Kumar D and Maiti M 2018 *Acta. Physica. Pol.* B **49** 687
[14] Blann M 1974 *Nucl. Phys.* A **235** 211
[15] Nandy M, Ghosh S and Sarkar P K 1999 *Phys. Rev.* C **60** 044607
[16] Maiti M and Lahiri S 2009 *Phys. Rev.* C **79** 024611
[17] Cavinato M, Fabrici E, Gadioli E, Erba E G, Vergani P, Crippa M, Colombo G, Redaelli I and Ripamonti M 1995 *Phys. Rev.* C **52** 2577
[18] Birattari C *et al* 1996 *Phys. Rev.* C **54** 3051
[19] Maiti M, Roy S N, Nandy M and Sarkar P K 2005 *Phys. Rev.* C **71** 034601
[20] Kumar D and Maiti M 2017 *Phys. Rev.* C **96** 044624
[21] Maiti M 2013 *J. Radioanal. Nucl. Chem.* **297** 319
[22] Maiti M 2013 *Radiochim. Acta* **101** 437
[23] Kumar D, Maiti M and Lahiri S 2017 *Sep. Sci. Technol.* **52** 2372
[24] Kumar D, Maiti M, Choudhury D and Lahiri S 2019 *Sep. Sci. Technol.* **54** 1661
[25] Maiti M and Lahiri S 2011 *Radiochim. Acta* **99** 359
[26] Maiti M and Lahiri S 2015 *Radiochim. Acta* **103** 7
[27] Maiti M, Datta A and Lahiri S 2015 *RSC Adv.* **5** 80919
[28] Kumar D, Maiti M and Lahiri S 2017 *Phys. Rev.* C **96** 014617
[29] Maiti M and Lahiri S 2011 *Phys. Rev.* C **84** 067601
[30] Maiti M 2011 *Phys. Rev.* C **84** 044615
[31] Maiti M and Lahiri S 2010 *Phys. Rev.* C **81** 024603
[32] Chauhan A and Maiti M 2019 *Phys. Rev.* C **99** 034608
[33] Chauhan A, Maiti M and Lahiri S 2019 *Phys. Rev.* C **99** 064609
[34] Comparetto G and Qaim S M 1980 *Radiochim. Acta* **27** 177
[35] Zaitseva N G, Stegailov V I, Khalkin V A, Shakun N G, Shishlyannikov P T and Bukov K G 1996 *Appl. Radiat. Isot.* **47** 145
[36] Ditrói F, Tárkányi F, Takács S, Hermanne A, Ignatyuk A V and Baba M 2012 *Nucl. Instrum. Methods Phys. Res.* B **270** 61
[37] Ismail M, Sharma R P and Rashid M H 1998 *Phys. Rev.* C **57** 1290
[38] Sudár S, Cserpák F and Qaim S M 2002 *Appl. Radiat. Isot.* **56** 821
[39] Ziegler J F, Ziegler M D and Biersack J P 2010 *Nucl. Instrum. Methods Phys. Res.* B **268** 1818
[40] Herman M, Capote R, Carlson B V, Obložinský P, Sin M, Trkov A, Wienke H and Zerkin V 2007 *Nucl. Data Sheets* **108** 2655
[41] Hauser W and Feshbach H 1952 *Phys. Rev.* C **87** 366
[42] Raynal J 1972 Optical-model and coupled-channel calculations in nuclear physics *International Atomic Energy Agency Report* http://inspirehep.net/record/19572/files/sti-pub-306.pdf#page=291
[43] Gilbert A and Cameron A G W 1965 *Can. J. Phys.* **43** 1446
[44] Ignatyuk A V, Weil J L, Raman S and Kahane S 1993 *Phys. Rev.* C **47** 1504
[45] D'Arrigo A, Giardina G, Herman M, Ignatyuk A V and Taccone A 1994 *J. Phys.* G **20** 365
[46] National Nuclear Data Center, Brookhaven National Laboratory, http://nndc.bnl.gov/nudat2/
[47] Blann M 1996 *Phys. Rev.* C **54** 1341
[48] Weisskopf V F and Ewing D H 1940 *Phys. Rev.* **57** 472
[49] Blann M 1971 *Phys. Rev. Lett.* **27** 337
[50] Blann M and Vonach H K 1983 *Phys. Rev.* C **28** 1475
[51] Musthafa M M, Singh B P, Sankaracharyulu M G V, Bhardwaj H D and Prasad R 1995 *Phys. Rev.* C **52** 3174
[52] Wang M, Audi G, Kondev F G, Huang W J, Naimi S and Xu X 2017 *Chin. Phys.* C **41** 030003
[53] Myers W D and Swiatecki W J 1967 *Ark. Phys.* **36** 343 https://escholarship.org/uc/item/3g69c9s2
[54] Becchetti F D Jr and Greenlees G W 1969 *Phys. Rev.* **182** 1190
[55] Bodansky D 1962 *Annu. Rev. Nucl. Sci.* **12** 79